Magnetoresistance, Gating and Proximity Effects in Ultrathin NbN-Bi$_2$Se$_3$ Bilayers

Gad Koren

Department of Physics, Technion—Israel Institute of Technology, Haifa 32000, Israel; gkoren@physics.technion.ac.il

Abstract: Ultrathin Bi$_2$Se$_3$-NbN bilayers comprise a simple proximity system of a topological insulator and an s-wave superconductor for studying gating effects on topological superconductors. Here we report on 3 nm thick NbN layers of weakly connected superconducting islands, overlayed with 10 nm thick Bi$_2$Se$_3$ film which facilitates enhanced proximity coupling between them. Resistance versus temperature of the most resistive bilayers shows insulating behavior but with signs of superconductivity. We measured the magnetoresistance (MR) of these bilayers versus temperature with and without a magnetic field H normal to the wafer (MR = [R(H) − R(0)]/{[R(H) + R(0)]/2}), and under three electric gate-fields of 0 and ±2 MV/cm. The MR results showed a complex set of gate sensitive peaks which extended up to about 30 K. The results are discussed in terms of vortex physics, and the origin of the different MR peaks is identified and attributed to flux-flow MR in the isolated NbN islands and the different proximity regions in the Bi$_2$Se$_3$ cap-layer. The dominant MR peak was found to be consistent with enhanced proximity induced superconductivity in the topological edge currents regions. The high temperature MR data suggest a possible pseudogap phase or a highly extended fluctuation regime.

Keywords: superconductivity; topological Insulator; thin films; bilayers; proximity effect; magnetoresistance

PACS: 73.20.-r; 73.43.-f; 85.75.-d; 74.90.+n

1. Introduction

Surface edge states of topological superconductors (TOS) are expected to support zero energy modes or Majorana fermions which are robust against disorder and decoherence [1,2]. These zero energy excitations could therefore be useful in potential application in spintronics and quantum computing [3,4]. Bulk TOS such as copper doped Bi$_2$Se$_3$ should have been the simplest materials to study TOS properties, but complications due to their inherent inhomogeneity [5] and the presence of possible superconducting impurity phases such as CuSe$_2$ [6], make them less attractive for such investigations. Recently, however, bulk superconducting PbTaSe$_2$ with T_c of 3.8 K was found to have zero energy states at vortices which is a hallmark of TOS [7]. An alternative way for realizing TOS is by inducing superconductivity in a topological insulator or in semiconductor-nanowires with strong spin-orbit interaction via the proximity effect (PE) [8–11]. Unconventional superconductivity in these systems, such as revealed by the presence of zero bias conductance peaks (ZBCP), indicates zero energy bound states that might be due to Majorana zero energy modes, but could also originate in zero energy Andreev bound states in an unconventional superconductor. It is hard to distinguish between these two different phenomena, and efforts are ongoing in order to achieve this goal [12,13].

Spatial sharpness of the boundary region between the superconductor and the topological or semi-conducting material is also essential in order to distinguish between the near-zero-energy end

states originating in Andreev bound states, and the Majorana zero energy modes in the topological case [14]. Since this boundary is generally created by gating in the experiments, its unavoidable gradual spatial change adds more uncertainty to the interpretation of the observed ZBCPs as due to the Majorana modes [10,11,15]. The role of gating in these nanowire-superconductor experiments was further investigated and a variety of additional phenomena such as ZBCP oscillations versus gate voltage and magnetic field were observed and interpreted in the context of Majorana modes as well as alternatives such as Kondo and disorder effects [16]. Hence, gating is sufficiently important in these studies and we decided to use a simple proximity system of a bilayer comprising of a topological insulator and a 2D superconductor for studying gating effects on topological superconductors [17]. In continuation to our previous studies of Bi_2Se_3-NbN junctions [18,19] we used ultra-thin bilayers of this system, even thinner than used before [17], where the superconducting NbN islands with weak-links in between them are overlayed with a thicker Bi_2Se_3 layer which enhances the coupling between the NbN islands via the proximity effect. Here we report on gating effects on the magnetoresistance (MR) of this hybrid system, which shows a highly gate sensitive, non-monotonous behavior versus temperature.

2. Experimental

2.1. Choice of the Bilayer Parameters

Here we explain why a highly resistive 10 nm thick Bi_2Se_3 on 3 nm thick NbN bilayer was chosen for presentation. It turned out that the R and MR results of similar but less resistive bilayers, showed that the MR above T_c was very similar to that of a bare 10 nm Bi_2Se_3 film (see Figure S2 of the supplementary material). This was a direct result from the fact that the links between superconducting islands of the 3 nm reference NbN film were still too strong, as is obvious from the almost full transition to zero resistance at low temperatures in Figure S1. We therefore had to weaken the inter-grain links even more. Since the use of 2.5 nm thick NbN films on Fused Silica (FS) yielded very resistive films, with R over a MΩ at low temperatures, with a lot of noise and a very weak signature of a transition at 2–3 K, we decided to stick with the 3 nm thick films in the bilayers. We thus prepared and characterized 7 wafers with the 10 nm Bi_2Se_3 on 3 nm NbN bilayers, and found out that their maximum resistance (at low temperatures) varied between about 1 and 10 kΩ. This depended mostly on the base pressure used before the deposition process (1.5×10^{-7}–3×10^{-7} Torr), but probably also on the surface quality of the FS wafers. In any case, the most significant results were obtained with the highest resistance bilayers, and here we present the results on the most resistive one, which also has the weakest links as we originally planned to have.

2.2. Surface Morphology of the Film and Bilayer

Figure 1a shows an atomic force microscope (AFM) image of the surface morphology of a 3 nm thick NbN film. A typical line height profile is shown in Figure 1b along the line in Figure 1a. While the lateral size of the NbN grains is ∼50–100 nm, one can see larger bright areas of at least 1000 nm in size which represent thicker superconducting NbN islands. These are separated by broad darker areas which constitute thinner weak-links between these islands. This islands structure that comprises a network of strong superconducting regions connected by weak-links is essential for the present study, otherwise a superconducting short will mask all our transport data. SEM images of similar NbN films on glass showing their grainy nature can also be seen in [20]. In addition, Figure 1a shows a few 1–3 nm deep holes of about 60 nm diameter while the overall rms roughness of this film is ∼0.35 nm.
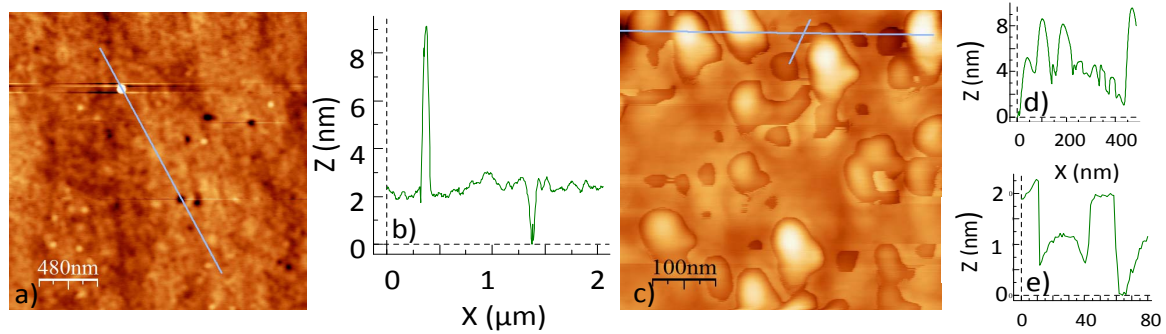
**Figure 1.** Atomic force microscope (AFM) images and line height profiles. (**a**) Image of nominally 3 nm thick NbN layer; (**b**) A line height profile along the line shown in (**a**); (**c**) Image of a 10 nm Bi_2Se_3 on a 3 nm NbN bilayer; (**d**,**e**) are two line height profiles along the long and short lines shown in (**c**), respectively.

Figure 1c shows an AFM image of the surface morphology of a 10 nm Bi_2Se_3 on a 3 nm NbN bilayer bilayer, together with two line height profiles in Figure 1d,e along the long and short lines shown in Figure 1c, respectively. The bilayer shows taller grains on a smoother background, with grains height of 4–8 nm and some holes, the deepest of which is of about 5 nm deep. Shallower holes are also visible which reveal a step-like depth profile as seen in Figure 1e, where the step heights are of about 1 or 2 nm in agreement with one or two quintuples of the Bi_2Se_3 structure. The overall rms roughness of this bilayer is ∼1.1 nm.

2.3. The Gates and Contacts Geometry

Figure 2a depicts a schematic drawing of the bilayer, gates positions and 20 representative contacts. Contacts C1 and C10 are separated from the bilayer by two scratches, while the 4 contacts of each are shorted and connected to the top and bottom gates, respectively. Since the fused silica substrate is 1.5 mm thick and its dielectric constant is low, the bottom gate is useless here and is shorted to the bilayer and ground, as can be seen in the schematic cross-section of the bilayer and gates in Figure 2b. The insulation layer of the top gate is made of a much thinner PMMA resist of 1.3 μm thickness which is painted and backed at 100 °C for 10 min. This allows for an electric field of ±2 MV/cm to be obtained when a voltage of ∓100 V is applied to the top gate (opposite polarity). This will be marked in the following by Vg = ∓100 V. Figure 2b shows two weakly connected NbN islands (red dots) together with the accumulation layer (blue dots on white background) in the Bi_2Se_3 layer near the interface with the NbN islands. Proximity induced superconductivity also occurs in this layer and can extend up to the top surface of the Bi_2Se_3 film [17]. We note that generally a depletion layer forms at the interface of a metal electrode in contact with a semiconductor provided $\phi_m > \phi_s$ where ϕ_m and ϕ_s are the work functions of the metal and the semiconductor, respectively [21]. Here however, the opposite case occurs and an accumulation layer forms since $\phi_m < \phi_s$ where the metallic NbN layer has $\phi_m = 4.7$ V [22] and the "semiconductor" Bi_2Se_3 layer $\phi_s = 5.6$ V [23]. The gate basically adds or removes charges from this accumulation layer. In a system similar to ours where bare Bi_2Se_3 thin films were investigated, Steinberg et al. describe different gating geometries and show how the depletion layer and energy bands change with the gate voltage [24,25]. Due to the much thinner dielectric used in these studies with its much higher dielectric constant, Steinberg et al. could reach electric fields of up to ±80 MV/cm while we could reach ±2 MV/cm only.
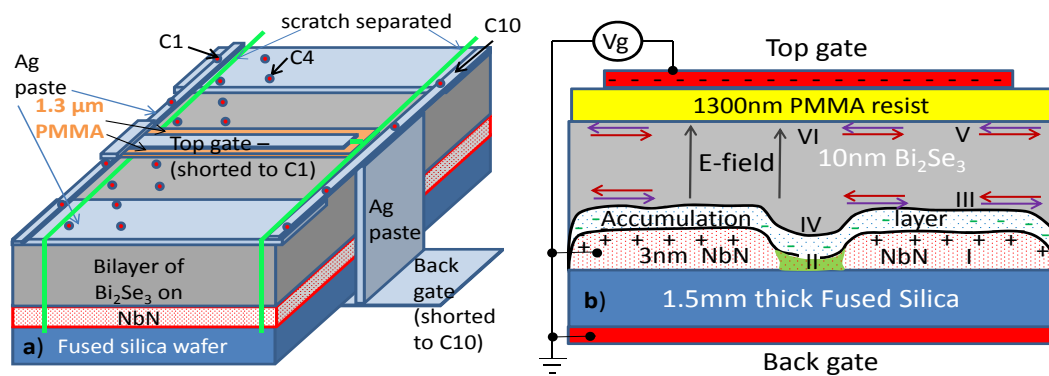
Figure 2. (**a**) A schematic drawing of the Bi_2Se_3 on NbN bilayer, together with the top and bottom gates and some of the Ci contacts where $i = 1$ to 10 (each Ci has 4-point contacts, the red dots along the y-direction). The C1 and C10 contacts are separated from the bilayer and dedicated for contacting the top and bottom gates, respectively; (**b**) A schematic model cross-section of the bilayer and gates. Two superconducting NbN islands, marked by the red-dots area, are weakly connected by the non-superconducting green shaded area. Helical edge currents for the two spin orientations of the Bi_2Se_3 layer are depicted by the horizontal arrows on the top and bottom surfaces. The accumulation layer in the Bi_2Se_3 is marked by the blue-dots area. The back gate is grounded and shorted to the bilayer in the present study, and a negative top gate voltage Vg = -100 V corresponds to a positive electric field E.

3. Results and Discussion

Figure 3 shows the resistance versus temperature of the 10 nm Bi_2Se_3 on 3 nm NbN on FS bilayer with the highest resistance at low temperatures. The temperature dependence of R clearly shows a dominant insulating behavior down to 2.5 K where a small decrease of resistance is observed. Similar behavior was observed also in 5 nm thin cuprate films [26]. We stress that the insulating behavior here is a result of transport via the weak-links connecting the NbN islands and is typical only of the highly resistive bilayers. In less resistive 3 nm thick NbN layers, as in Figure S1, R versus T shows metallic behavior and a clear transition to superconductivity. Thus the conjectured presence of a network of NbN islands connected by weak-link boundaries in our films (the darker areas in Figure 1a) is clearly demonstrated by the insulating behavior seen in Figure 3. We show data at four locations on the wafer which exhibits quite a spread, and also the data of contact C6 at 0 and 1 T magnetic field under Vg = 0 V. Clearly, the small decrease of R below 2.5 K disappears under 1 T, and we thus conclude that it originates in superconductivity of the NbN islands which are very weakly linked. The inset shows conductance spectra of all these contacts at 1.86 K which clearly exhibit tunneling behavior between the superconducting islands. The gap-like feature appearing at about 70 meV, is a result of several weak-links connected in series between the voltage contacts. Assuming an energy gap Δ of 2 meV for the NbN islands [27] yields 35 such weak-links in series. The dips in the conductance spectra of the inset are due to heating effects as a result of reaching the critical current in the weak-links connecting the NbN islands [28].

The main results of this study are presented in Figure 4 and its inset, where the MR of the bilayer of Figure 3 for 0 and 1 T and under different gate voltages shows a complex, non monotonous peaks structure. For comparison, the corresponding monotonous MR of the reference 10 nm Bi_2Se_3 film of Figure S2 is also shown. Below 2.5 K, the MR is similar to the results in the inset to Figure S1, but with a 3–5 times smaller signal at the maximum MR at ~1.9 K. The later reflects the fact that the weak-links here are much weaker than in Figure S1. There is also no visible effect of the gate voltage on the MR results in this regime. Above 2.5 K, the MR data becomes very sensitive to the gate voltage, and up to 7–8 K exhibit kind of anti-phase behavior versus temperature for Vg = ±100 V where the peak and dip at 3.5 K reverse roles at 6–7 K. The MR under Vg = 0 V is somewhere in between these two at 3.5 K, but

then becomes closer to the Vg = −100 V data at 6–7 K. At higher temperatures the MR data becomes even more complex, but clearly it goes down at 25–30 K, where it tends to follow the reference Bi_2Se_3 film. It should be stressed here that the MR behavior of Figure 4 for the C4 contact, was observed also for the other contacts on this wafer (C6 and C8), while C7 had an additional strong oscillatory behavior above 10 K as shown in Figure 5 for Vg = 0 V. This oscillatory behavior was washed out under either Vg = +100 V or Vg = −100 V. The inset to Figure 5 is a zoom-in on weaker oscillations or plateaus in the MR of C7 in the range of 3–8 K. Such plateaus and knees, although weaker, appear also in the other contacts. As far as we know, there is no theory that predicts oscillations of MR versus temperature in a 2D topological superconductor.
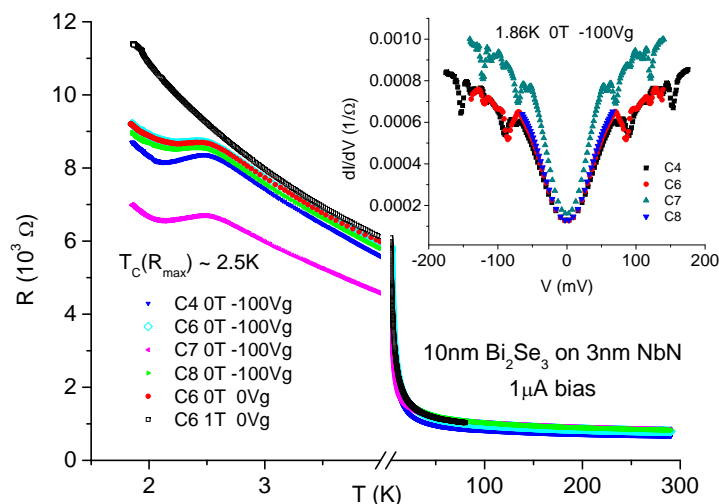
Figure 3. Resistance versus temperature of a pristine 10 nm Bi_2Se_3 on 3 nm NbN on FS bilayer under different magnetic fields and gate voltages. The inset shows conductance spectra of this highly resistive bilayer at 1.86 K, 0 T and Vg = −100 V.
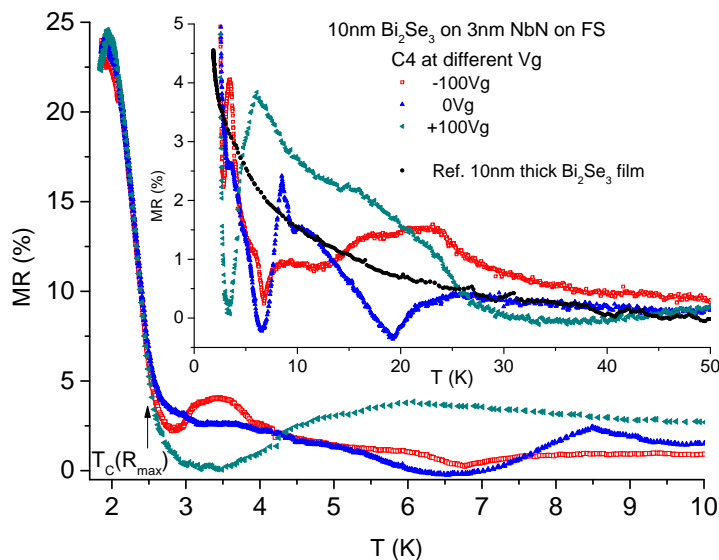

Figure 4. Magnetoresistance versus temperature of the C4 contact of the pristine bilayer of Figure 3, obtained for 0 and 1 T fields and under gate voltages Vg of 0 and ±100 V. All other contacts show similar behavior. The inset shows the full temperature range while the main panel is a zoom in on the low temperature regime. The inset also shows the magnetoresistance (MR) of the reference 10 nm thick Bi_2Se_3 film of Figure S2.
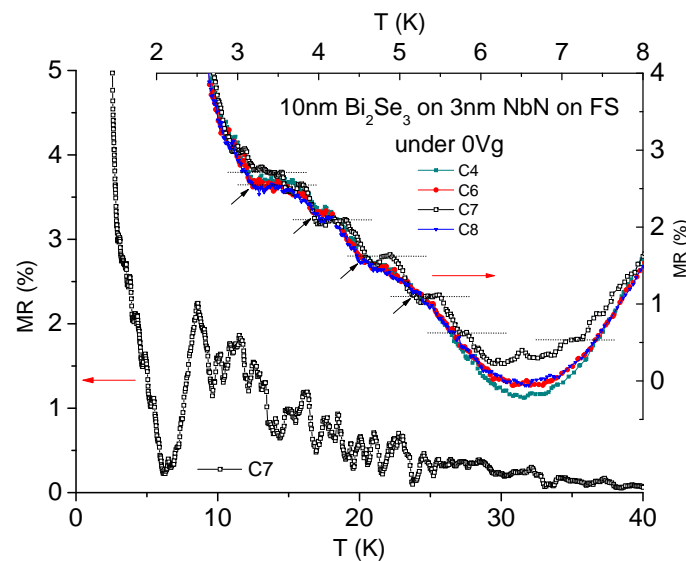
Figure 5. MR versus temperature at Vg = 0 V of the C7 contact on the wafer of Figure 3. The oscillations were smeared out under Vg = ±100 V. The inset is a zoom in on the data at low temperatures. Only this C7 contact showed the pronounced oscillations versus temperature, although plateaus and less pronounced knees were observed also in the other contacts as seen in the inset and marked by the arrows.

To find out whether these oscillations and plateaus originate in magnetic field effects, we measured R versus H for all the contacts on the wafer of Figure 3 at 1.85 K. The results are depicted in Figure 6a, and they are quite similar to those of the inset to Figure S2, besides the difference in overall resistance and aging effects. We have also measured R versus H under Vg = 0 V on this wafer (when it was 1.5 month old) at higher temperatures. A background of a polynomial of order 2 fit to the data was subtracted from the data, and the resulting resistance variation ΔR versus H was obtained. The normalized $\Delta R(H)/R(0)$ results at ~9.5 K are plotted in Figure 6b versus magnetic field. Presuming that the observed oscillations originate in flux quantization in nano-holes in the bilayer, we obtain from the period $\Delta H \sim 0.6$ T a hole diameter of 66 nm, which agrees quite well with the AFM image and line profile of the 3 nm thick NbN film of Figure 1a,b. This result suggests that superconductivity in the bilayer persists at least up to ~9.5 K. Similar oscillations were observed also in the other contacts at 3.7 and 5.3 K, but they disappeared at 15.1 K in the noise level of the measurements. Thus T_c of the NbN islands in this bilayer should be between 9.5 and 15.1 K. This is in agreement with the the MR onset in Figure S6 under 4 T (12.2 K), or the temperatures of maximum resistance of Figure S5 (12–13 K), although in that case the NbN film was 4 nm thick and not 3 nm thick as in the present bilayer. We conclude from these findings that T_c of the superconducting islands in our bilayer can reach 12–13 K, and that if fluctuations are taken into account, superconductivity could persist in our bilayers up to ~15 K. Thus, it should be possible to observe flux-flow effects of vortices up to this temperature, but this however, does not explain the non monotonous MR features observed in Figures 4 and 5. Above 15 K, any MR effect different from that due to the reference 10 nm Bi_2Se_3 film, should have a different origin.
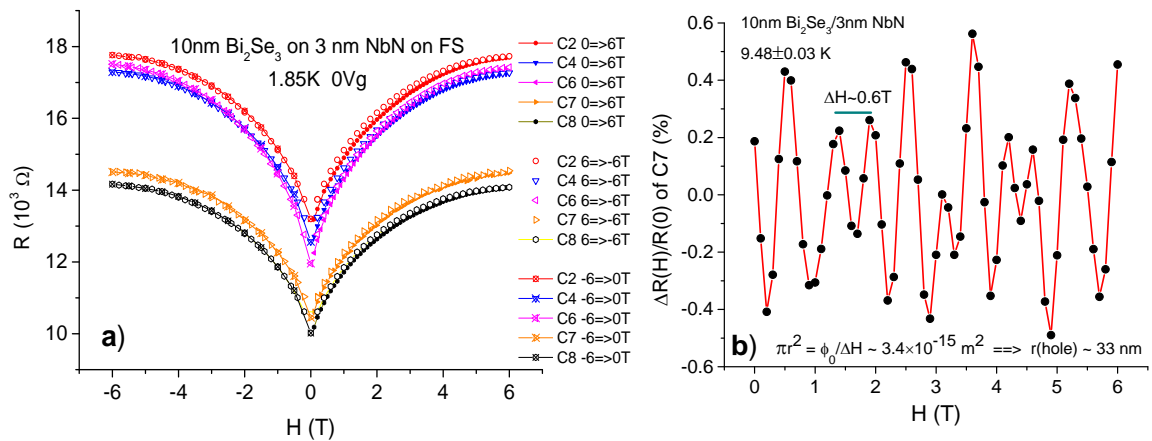
Figure 6. (**a**) Resistance versus magnetic field of the bilayer of Figure 3 at 1.85 K and Vg = 0 V. Although this bilayer was kept in dry air for one month prior to this measurement, it deteriorated (aged) as can be seen from the increase of its resistance values at 0 T by about 4 kΩ as compared to Figure 3; (**b**) Oscillations of normalized R minus background [ΔR(H)/R(0)] of the C7 contact of Figure 5 versus field at 9.48 K and Vg = 0 V.

Another possible origin of the oscillations seen in Figure 6b is the magnetic Aharonov–Bohm (AB) effect, as seen in mesoscopic DC SQUID loops made of Aluminum under fields above H_{c2} at 20 mK [29], and in graphene rings at 500 mK [30]. In addition to the tens of nm wide via-holes of the nominally 3 nm thick NbN layer seen in Figure 1a, one sees many small less dark dots and zones which signify thinner areas. These are not via-holes, but the insulating weak-links of the film, which are equivalent to shallow holes with much fewer electrons thus constituting the insulating centers of metallic loops. In this context, AB oscillations in the present bilayers are possible at low temperatures. However, the oscillations in Figure 6b are observed at quite a high temperature (about 9.5 K), which leads to a much smaller phase coherence of the normal electrons in the NbN layer. This makes it less likely that the AB effect is at the origin of the presently observed oscillation in the capped NbN layer versus the magnetic field. Nevertheless, Figure S3 of the supplementary shows that at 10 K the phase coherence lengths L_ϕ of a bare 10 nm thick Bi$_2$Se$_3$ film range between 50 and 120 nm. As a result, the AB effect is more plausible as the source of the observed oscillations if it originates in the Bi$_2$Se$_3$ layer of the bilayer. To verify which of the proposed scenarios raised in this study as the source for the observed oscillation in Figure 6b, further work is needed.

Next, we discuss possible explanations for the complex behavior of the MR results of Figure 4. In principle, the present bilayer as drawn schematically in Figure 2b, comprises of six distinct superconducting regions, marked in this figure by I to VI. The NbN islands (I) and the inter-islands regions (II) are the obvious ones, but proximity induced superconductivity occurs also in the Bi$_2$Se$_3$ layer above these regions, in particular, at the bottom and top surfaces of this doped topological layer where the helical edge currents flow. This yields four more superconductive regions in the cap Bi$_2$Se$_3$ layer, two above the islands (III and V) and two above the inter-islands regions (IV and VI). Due to proximity effect and distances from the superconducting NbN islands (I), we can safely assume that $T_c(I) > T_c(III) > T_c(II) > T_c(IV)$. We shall assume first that the MR results observed in Figure 4 originates in vortex physics, and discuss them in terms of pinning in the different superconducting regimes I–VI. Then, for the remaining unidentified features, we shall discuss possible contributions to the MR from zero energy Majorana modes and unconventional superconductivity.

In the context of vortex physics, the MR peaks seen in Figure 4 as a function of temperature originate in flux-flow, and are due to two competing phenomena. One is the increased vortex generation on cooling down due to newly formed proximity induced superconducting areas in the bilayer which eventually saturates, and the other is increased pinning with decreasing temperature. The result of these effects is an MR peak versus temperature below which all vortex motion stops and the MR goes

to zero. Such MR peaks have been clearly observed in similar cuprate bilayers [31], as well as in the inset to Figure S1. Since the bottom Bi_2Se_3 surface of regions III and IV are very close to regions I and II, the proximity induced superconductivity in them is stronger than in the more distant regions V and VI. We shall first discuss the MR versus T result of Figure 4 under Vg = 0 V. The MR of this data is most always lower than that of the reference Bi_2Se_3 film. This looks like MR suppression in the bilayer, but since there are zero MR regimes in the bilayer data (at 6–7 and 18–20 K), it looks more like an indication of strongly interacting layers in the bilayer. This interaction seems to play a lesser role only above 25 K where the two curves coincide, apparently because no superconductivity affects the MR results at this high temperature range. We attribute the double MR peak between 7–15 K to flux flow, vortex generation and pinning in regions I and III. We note here that the above analysis was facilitated by the fact that this double peak is fully separated from the other features of the MR curve. Using similar arguments, we can attribute the broad MR knee between 2.5 and 6.5 K to pinning in regions II, and the large MR peak below 2.5 K to pinning effects in region IV. The fact that the MR peak below 2.5 K is so strong might be due to enhance proximity induced superconductivity by the surface currents of the topological layer in region IV, or to additional contributions from other effects, to be discussed below.

We shall now analyze the MR results of Figure 4 under different gate voltages and try to explain the two prominent peaks at 3.5 and 6 K under Vg = −100 V and +100 V, respectively. We note that transport, and therefore also the MR data, is strongly dependent on the conductance of regions II and IV, since they comprise the weak-links for current flow in the bilayer. As a result, they will be more sensitive to gating than region III. Under Vg = 0 V, the accumulation layer in Figure 2b in between the NbN islands (region II), is negatively charged or simply electron rich. Once a −100 V is applied to the top gate, the NbN layer becomes positively charged and this removes electrons from the accumulation layer of region II, (as well as from the adjacent region IV just above it). Thus, the smaller electron density of region II lowers its T_c onset to about 4 K compared to its value without gating (onset at ∼6.5 K). The MR peak at 3.5 K under Vg =−100 V is consistent with this scenario, and therefore seems to originate in region II. The large MR peak at 1.9 K seems to be unaffected by either of the present gate voltages of Vg = ±100 V, and this again might originate in topological effects in region IV. Under Vg = +100 V, the accumulation layer becomes even richer with electrons as compared to its natural electron rich state under Vg = 0 V, thus the proximity induced T_c in region II is higher than the 4 K obtain before under Vg = −100 V. The MR peak at 6 K under Vg = +100 V can thus originate also in region II. Besides the two prominent peaks at 3.5 and 6 K, additional MR features under gating can be seen in Figure 4. These include the broad hump under Vg = +100 V between 10 and 25 K, and the broad peak between 15 and 30 K under Vg = −100 V. As discussed before, superconductivity dies off at about 15 K, and any proximity induced T_c will obviously be lower. Therefore, if one wishes to invoke vortex motion as the origin of these extra MR features, one has to assume the existence of a pseudogap phase for the present bilayers. Signature of such a phase was found in point contact conductance spectra measurements of copper doped $Cu_{0.2}Bi_2Se_3$ single crystals with $T_c \sim 3$ K, where a depletion of density of states at low bias was observed up to ∼20 K [32]. Considering that in the present bilayers the NbN islands have a much higher $T_c \sim$ 12–13 K, the conjectured pseudogap phase could easily reach 25–30 K. Hence, to summarize, the extra MR features in Figure 4 above 15 K could originate in flux flow, provided a pseudogap phase exists in our system. In the cuprates, where the pseudogap phase is well established, such vortices were detected in thermoelectric measurements under a magnetic field (the Nernst effect) [33].

Finally, we focus on the intensity or magnitude of the MR peaks in Figure 4, and on what might contribute extra strength to the dominant peak at 1.9 K. We note that the volume fraction of the superconducting NbN islands with the highest T_c values is apparently very small, as can be inferred from the very small resistive transition at 2.5 K in Figure 3. Previously, in the vortex pinning context, we attributed the MR double peak under Vg = 0 V at 7–15 K to regions I and III, the knee between 2.5 and 6.5 K to region II, and the large MR peak below 2.5 K to region IV. It was hard to reconcile how region IV, with its presumably weakest superconductivity, leads to such a large MR peak. Thus, if the

enhanced MR peak at 1.9 K is still due to pinning effects, we are led to the conclusion that region IV must have enhanced superconductivity just as well. Such enhancement might originate in a longer normal coherence length ξ_N in the Bi$_2$Se$_3$ at low temperatures, which is possibly enhanced further by hybridization of the helical surface currents of regions IV and VI. We know of no theory that predicts such effects, and therefore this interpretation is only a hypothesis at the present time. An alternative scenario for the interpretation of our results is that the MR knee between 2.5 and 6.5 K is due to pinning effects in both region II and region IV. This would leave the dominant MR peak at 1.9 K unaccounted for, and other effects as for its origin should be explored. But this time, vortices in the bilayer are fully pinned and presumably form a vortex lattice. Vortices in general, in a topological superconductor, are predicted to host zero energy Majorana modes in the vortex cores [2]. Thus, in a dense periodic vortex lattice, interactions between these modes lead to the creation of new energy bands in the band gap of this system, some of which could be quite flat [34]. Whether or not these Majorana bands contribute to the MR of the bilayer is unknown at the present time. Rigorous MR calculation versus temperature are needed in order to test if this scenario actually occurs in the present bilayers.

4. Materials and Methods

The NbN and Bi$_2$Se$_3$ thin films were prepared as described in detail previously [17]. Briefly, laser ablation deposition was used where the NbN films were deposited under 30 mTorr of N$_2$ gas flow and at 600 °C heater block temperature, while the Bi$_2$Se$_3$ layers were deposited under vacuum and at 300 °C. All films and bilayers were deposited on fused silica wafers and yielded grainy films with rms roughness of ∼10% of the films thickness. All the Bi$_2$Se$_3$-NbN bilayers in the present study were obtained using an "in-situ" process where both the 3 nm thick NbN film and the 10 nm thick Bi$_2$Se$_3$ cap layer were prepared in the same deposition run without breaking the vacuum. This kept the interface between the NbN and Bi$_2$Se$_3$ layers protected against contamination and oxidation which occur if the NbN surface is exposed to air [17,35]. Transport measurements were done using an array of 40 gold coated spring loaded spherical tips for the 4-probe measurements on 10 different locations on the wafer (Ci with $i = 1$–10, 4 contacts for each location).

5. Conclusions

A comprehensive study of ultra thin bilayers comprising of weakly connected s-wave superconducting islands and a continuous topological insulator cap-layer reveal interesting gate and temperature dependent magnetoresistance features. These features could be explained as originating in vortex physics, where proximity induced superconductivity and pinning effects in the different regions of the bilayer play a major role. In particular, the present results are consistent with enhanced superconductivity in the surface region of the topological layer in contact with the superconductor, where the helical edge currents flow. Signature of a pseudogap was found, and a possible contribution to the data from Majorana bands was discussed.

References

1. Hassan, M.Z.; Kane, C.L. Colloquium: Topological insulators. *Rev. Mod. Phys.* **2010**, *82*, 3045–3067.
2. Fu, L.; Kane, C.L. Superconducting Proximity Effect and Majorana Fermions at the Surface of a Topological Insulator. *Phys. Rev. Lett.* **2008**, *100*, 096407.
3. Pesin, D.; MacDonald, A.H. Spintronics and pseudospintronics in graphene and topological insulators. *Nat. Mater.* **2012**, *11*, 409–416.
4. Bravyi, S.B.; Kitaev, A. Fermionic quantum computation. *Ann. Phys.* **2002**, *298*, 210–226.

5.   Kriener, M.; Segawa, K.; Ren, Z.; Sasaki, S.; Wada, S.; Kuwabata, S.; Ando, Y. Electrochemical synthesis and superconducting phase diagram of $Cu_xBi_2Se_3$. *Phys. Rev. B* **2011**, *84*, 054513.

6.   Ando, Y. Topological insulator materials. *J. Phys. Soc. Jpn.* **2013**, *82*, 102001.

7.   Guan, S.Y.; Chen, P.J.; Chu, M.W.; Sankar, R.; Chu, F.; Jeng, H.T.; Chang, C.S.; Chuang, T.M. Superconducting topological surface states in the noncentrosymmetric bulk superconductor $PbTaSe_2$. *Sci. Adv.* **2016**, *2*, e1600894.

8.   Koren, G.; Kirzhner, T.; Lahoud, E.; Chashka, K.B.; Kanigel, A. Proximity induced superconductivity by Bi in topological Bi_2Te_2Se and Bi_2Se_3 films: Evidence for a robust zero energy bound state that could be due to Majorana Fermions. *Phys. Rev. B* **2011**, *84*, 224521.

9.   Yang, F.; Ding, Y.; Qu, F.; Shen, J.; Chen, J.; Wei, Z.; Ji, Z.; Liu, G.; Fan, J.; Yang, C.; et al. Proximity effect at superconducting Sn-Bi_2Se_3 interface. *Phys. Rev. B* **2012**, *85*, 104508.

10.   Mourik, V.; Zuo, K.; Frolov, S.M.; Plissard, S.R.; Bakkers, E.P.; Kouwenhoven, L.P. Signatures of Majorana fermions in hybrid superconductor-semiconductor nanowire devices. *Science* **2012**, *336*, 1003.

11.   Das, A.; Ronen, Y.; Most, Y.; Oreg, Y.; Heiblum, M.; Shtrikman, H. Zero-bias peaks and splitting in an Al-InAs nanowire topological superconductor as a signature of Majorana fermions. *Nat. Phys.* **2012**, *8*, 887–895.

12.   Xu, J.P.; Liu, C.; Wang, M.X.; Ge, V.; Liu, Z.L.; Yang, X.; Chen, Y.; Liu, Y.; Xu, Z.A.; Gao, C.L.; et al. Artificial topological superconductor by the proximity effect. *Phys. Rev. Lett.* **2014**, *112*, 217001.

13.   Haim, A.; Berg, E.; von Oppen, F.; Oreg, Y. Signatures of Majorana zero modes in spin-resolved current correlations. *Phys. Rev. Lett.* **2015**, *114*, 166406.

14.   Kells, G.; Meidan, D.; Brouwer, P.W. Near-zero-energy end states in topologically trivial spin-orbit coupled superconducting nanowires with a smooth confinement. *Phys. Rev. B* **2012**, *86*, 100503.

15.   Higginbotham, A.P.; Albrecht, S.M.; Kirsanskas, G.; Chang, W.; Kuemmeth, F.; Krogstrup, P.; Jespersen, T.S.; Nygard, J.; Flensberg, K.; Marcus, C.M. Parity lifetime of bound states in a proximitized semiconductor nanowire. *Nat. Phys.* **2015**, *11*, 1017–1021.

16.   Churchill, H.O.H.; Fatemi, V.; Grove-Rasmussen, K.; Deng, M.T.; Caroff, P.; Xu, H.Q.; Marcus, C.M. Superconductor-nanowire devices from tunneling to the multichannel regime: Zero-bias oscillations and magnetoconductance crossover. *Phys. Rev. B* **2013**, *87*, 241401.

17.   Koren, G. Proximity effects at the interface of a superconductor and a topological insulator in NbN-Bi_2Se_3 thin film bilayers. *Supercond. Sci. Technol.* **2015**, *28*, 025003.

18.   Koren, G.; Kirzhner, T. Zero-energy bound states in tunneling conductance spectra at the interface of an s-wave superconductor and a topological insulator in NbN/Bi_2Se_3/Au thin-film junctions. *Phys. Rev. B* **2012**, *86*, 144508.

19.   Koren, G.; Kirzhner, T.; Kalcheim, Y.; Millo, O. Signature of proximity-induced px + ipy triplet pairing in the doped topological insulator Bi_2Se_3 by the s-wave superconductor NbN. *EPL* **2013**, *103*, 67010.

20.   Du, X.-K.; Wang, T.-M.; Wang, C.; Chen, B.L.; Zhou, L. Microstructure and Optical Characterization of Magnetron Sputtered NbN Thin Films. *Chin. J. Aeronaut.* **2007**, *20*, 140–144.

21.   Zhang, Z.; Yates, J.T., Jr. Band bending in semiconductors: Chemical and physical consequences at surfaces and interfaces. *Chem. Rev.* **2012**, *112*, 5520–5551.

22.   Gotoh, Y.; Tsuji, H.; Ishikawa, J. Measurements of work function of transition metal nitride and carbide thin films. *J. Vac. Sci. Technol. B* **2003**, *21*, 1607.

23.   Takane, D.; Souma, S.; Sato, T.; Takahashi, T.; Segawa, K.; Ando, Y. Work function of bulk insulating topological-insulator $Bi_{2-x}Sb_xTe_{3-y}Se_y$. *Appl. Phys. Lett.* **2016**, *109*, 91601.

24.   Steinberg, H.; Gardner, D.J.; Lee, Y.S.; Jarillo-Herrero, P. Surface state transport and ambipolar electric field effect in Bi_2Se_3 nanodevices. *Nano Lett.* **2010**, *10*, 5032–5036.

25.   Steinberg, H.; Laloe, J.-B.; Fatemi, V.; Moodera, J.S.; Jarillo-Herrero, P. Electrically tunable surface-to-bulk coherent coupling in topological insulator thin films. *Phys. Rev. B* **2011**, *84*, 233101.

26.   Koren, G.; Millo, O. Conventional proximity effect in bilayers of superconducting underdoped $La_{1.88}Sr_{0.12}CuO_4$ islands coated with nonsuperconducting overdoped $La_{1.65}Sr_{0.35}CuO_4$. *Phys. Rev. B* **2009**, *80*, 054507.

27.   Kamlapure, A.; Mondal, M.; Chand, M.; Mishra, A.; Jesudasan, J.; Bagwe, V.; Benfatto, L.; Tripathi, V.; Raychaudhuri, P. Measurement of magnetic penetration depth and superconducting energy gap in very thin epitaxial NbN films. *Appl. Phys. Lett.* **2010**, *96*, 072509.

28. Sheet, G.; Mukhopadhyay, S.; Raychaudhuri, P. Role of critical current on the point-contact Andreev reflection spectra between a normal metal and a superconductor. *Phys. Rev. B* **2004**, *69*, 134507.

29. Oudenaarden, A.; Devoret, M.H.; Nazarov, Y.V.; Mooij, J.E. Magneto-electric Aharonov-Bohm effect in metal rings. *Nature* **1998**, *391*, 768–770.

30. Huefner, M.; Molitor, M.; Jacobsen, A.; Pioda, A.; Stampfer, C.; Ensslin, K.; Ihn, T. The Aharonov-Bohm effect in side-gated graphene ring. *New J. Phys.* **2010**, *12*, 043054.

31. Koren, G.; Millo, O. Enhancement of the superconducting transition temperature of $La_{2-x}Sr_xCuO_4$ and $La_{1.875}Ba_{0.125}CuO_4$ bilayers: Bilayer and reference film prepared on the same wafer. *Phys. Rev. B* **2010**, *81*, 134516.

32. Kirzhner, T.; Lahoud, E.; Chaska, K.B.; Salman, Z.; Kanigel, A. Point-contact spectroscopy of $Cu_{0.2}Bi_2Se_3$ single crystals. *Phys. Rev. B* **2012**, *86*, 064517.

33. Wang, Y.; Li, L.; Ong, N.P. Nernst effect in high-T_c superconductors. *Phys. Rev. B* **2006**, *73*, 024510.

34. Liu, T.; Franz, M. Electronic structure of topological superconductors in the presence of a vortex lattice. *Phys. Rev. B* **2015**, *92*, 134519.

35. Darlinski, A.; Halbritter, J. Angle-resolved XPS Studies of Oxides at NbN, NbC, andl Nb Surfaces *Surf. Interface Anal.* **1987**, *10*, 223–237.